Revista Integración
Escuela de Matemáticas
Universidad Industrial de Santander
Vol. 29, No. 1, 2011, pág. 59–72

Timelike and null equatorial geodesics in the Bonnor-Sackfield relativistic disk

Guillermo A. González[a,*], Framsol López-Suspes[a,b]

[a] Universidad Industrial de Santander, Escuela de Física, Bucaramanga, Colombia.

[b] Universidad Santo Tomás, Facultad de Telecomunicaciones, Bucaramanga, Colombia.

Abstract. A study of timelike and null equatorial geodesics in the Bonnor-Sackfield relativistic thin disk is presented. The motion of test particles in the equatorial plane is analyzed, both for the newtonian thin disk model as for the corresponding relativistic disk. The nature of the possible orbits is studied by means of a qualitative analysis of the effective potential and by numerically solving the motion equation for radial and non-radial equatorial trajectories. The existence of stable, unstable and marginally stable circular orbits is analyzed, both for the newtonian and relativistic case. Examples of the numerical results, obtained with some simple values of the parameters, are presented.
Keywords: General relativity, exact solutions, equations of motion.
MSC2000: 83Cxx, 83C10, 83C15.

Geodésicas tipo tiempo y nulas en el plano ecuatorial del disco relativista de Bonnor-Sackfield

Resumen. En este trabajo se presenta un estudio de las geodésicas temporales y nulas en el disco delgado relativista y newtoniano de Bonnor-Sackfield. Se analiza el movimiento de las partículas de prueba en el plano ecuatorial, tanto para el modelo newtoniano del disco delgado como para el disco relativista correspondiente. La naturaleza de las órbitas posibles se estudia por medio de un análisis cualitativo del potencial efectivo, y numéricamente mediante la solución de la ecuación de movimiento de las trayectorias ecuatorial radial y no radial: Se analiza la existencia de órbitas estables, circulares inestables y estables marginalmente, tanto para el caso newtoniano, como el relativista. Se presentan ejemplos de los resultados numéricos obtenidos con algunos valores de los parámetros simples.
Palabras claves: Relatividad general, soluciones exactas, ecuaciones de movimiento.

*Corresponding author: *E-mail*: guillego@uis.edu.co
Received: 11 March 2010, accepted: 3 June 2011.

1. Introduction

Stationary or static axially symmetric exact solutions of Einstein equations corresponding to relativistic thin disks are of great astrophysical relevance since they can be used as models of certain stars, galaxies and accretion disks. These were first studied by Bonnor and Sackfield [5], obtaining pressureless static disks, and then by Morgan and Morgan, obtaining static disks with and without radial pressure [18, 19]. Several classes of exact solutions of the Einstein field equations corresponding to static thin disks with or without radial pressure have been obtained by different authors [16, 17, 15, 11, 12, 3, 4, 13, 14, 9, 7]. Also stationary thin disks have been obtained [2, 8], with or without radial pressure and heat flow.

Closely related with the above study is the analysis of the motion of test particles in the gravitational field generated by such disklike distributions of matter. In particular, the study of orbits in the equatorial plane is of clear astrophysical relevance, due to its relation with the dynamics of intergalactic stellar motion or the flow of particles in accretion disks around black holes. However, in spite of this, literature about this subject is rather scarce [23, 22, 21, 6]. Now, between the known relativistic static thin disks, the family of Bonnor-Sackfield [5] and Morgan-Morgan [18] solutions deserves special attention as they are of finite extension, and so they can be considered as appropriated relativistic flat galaxy models. On the other hand, the Morgan-Morgan disk with $n = 0$ corresponds to the Bonnor-Sackfield solution, which describes a finite relativistic thin disk whose surface mass density is singular at the rim [5, 7].

In agreement with the above considerations, we began with this paper a study of the equatorial geodesics in the Morgan-Morgan disks. We consider in this paper the $n = 0$ case, the Bonnor-Sackfield disk, as this is the simplest member of the family and also because this member of the family have a behavior qualitatively different from the others. The paper is organized as follows. First, in section 2, we present the Bonnor-Sackfield solution and the surface densities of mass and energy of the corresponding newtonian and relativistic disk models. Then, in section 3, we analyze the motion of test particles in the equatorial plane of the newtonian thin disk model and, in section 4, the motion of test particles in the corresponding relativistic thin disk model. Finally, in section 5, we summary our main results.

2. The Bonnor-Sackfield solution

The metric for a static axially symmetric spacetime can be written as the Weyl line element [25, 26, 10]

$$ds^2 = -e^{2\psi}dt^2 + e^{-2\psi}[\rho^2 d\varphi^2 + e^{2\gamma}(d\rho^2 + dz^2)], \tag{1}$$

where γ and ψ are functions of ρ and z only. The Einstein vacuum equations for this metric are

$$\psi_{,\rho\rho} + \frac{1}{\rho}\psi_{,\rho} + \psi_{,zz} = 0, \tag{2}$$

$$\gamma_{,\rho} = \rho\left(\psi_{,\rho}^2 - \psi_{,z}^2\right), \tag{3}$$

$$\gamma_{,z} = 2\rho\psi_{,\rho}\psi_{,z}, \tag{4}$$

the well known Weyl equations. Note that (2) is the Laplace equation in flat three-dimensional space, and so ψ can be taken as a solution of Laplace equation for an appropriated newtonian source with axial symmetry. Once a solution ψ is known, γ is easily computed from (3) and (4).

We introduce now the oblate spheroidal coordinates, whose symmetry adapts in a natural way to a finite thin disk. This coordinates are related to the usual cylindrical coordinates by the relation [20]

$$\rho^2 = (1+u^2)(1-v^2), \tag{5}$$

$$z = uv, \tag{6}$$

where $0 \leq u < \infty$ and $-1 \leq v \leq 1$. The disk is located at $z = 0$, $0 \leq \rho \leq 1$, so that $u = 0$ and $0 \leq v^2 < 1$. As we can see, on crossing the disk v changes sign but does not change in absolute value. This singular behavior of the coordinate v implies that an even function of v is a continuous function everywhere but has a discontinuous normal derivative at the disk. Then, the Einstein equations yield an energy-momentum tensor $T_{\alpha\beta} = S_{\alpha\beta}\ \delta(z)$ that leads to the interpretation of this solution as a thin disk (see, for instance, [9, 7]). Although the radius of the disk has been taken as one, a suitable re-scaling of ρ can be made in order to obtain expressions for disks with arbitrary radius: we only need to make the transformation $\rho \to a\rho$, where a is the radius of the disk.

A simple solution of the Weyl equations (2)-(4), obtained independently by Zipoy [27] and Vorhees [24] and interpreted by Bonnor and Sackfield [5] as the gravita-

tional field of a pressureless static thin disk, is given by

$$\psi = -m \cot^{-1} u, \tag{7}$$

$$\gamma = -\frac{m^2}{2} \ln \left[\frac{u^2+1}{u^2+v^2} \right], \tag{8}$$

where ψ is the newtonian gravitational potential of a thin disk with surface mass density given by [1]

$$\sigma_N = \frac{m}{2\pi\sqrt{1-r^2}}, \tag{9}$$

whereas that ψ and γ leads to a relativistic dust disk with surface energy density given by [5, 7]

$$\sigma = \frac{4me^{-m\pi/2}}{(1-r^2)^{(m^2+1)/2}}. \tag{10}$$

Here m is the mass of the disk and we are taking units where $G = 1$. From (9) and (10) we can see that the mass and energy densities are singular at the rim of the disk. However, as the energy density is positive everywhere, the energy-momentum tensor of the disk agrees with all the energy conditions.

Now, from the four-acceleration of a test particle, we can see that

$$\dot{U}_\mu = \frac{1}{2} g_{\alpha\beta,\mu} U^\alpha U^\beta, \tag{11}$$

where U^μ is the four-velocity of the particle and $\dot{U}_\mu = dU_\mu/d\tau$. Accordingly, for any static axially symmetric spacetime the only nonzero components of $\dot{U}_\mu$ are $\dot{U}_\rho$ and $\dot{U}_z$. Furthermore, the reflectional symmetry of the thin disk solutions with respect to the equatorial plane, the $z = 0$ plane, implies that $g_{\mu\nu,z}|_0 = 0$ and thus a particle that initially moves at the equatorial plane, it will remains in this plane. In agreement with this, we will consider only motion restricted to the equatorial plane.

3. The Newtonian motion

We now analyze the motion of test particles in the equatorial plane of the newtonian thin disk with gravitational potential given by (7). In order to do this, we began with the motion equation

$$\frac{d^2\mathbf{x}}{d^2t} = -\nabla\psi, \tag{12}$$

where $\mathbf{x} = (\rho, z)$. New, as is well known, there are two motion integrals, the specific angular momentum about the z-axis, ℓ, and the specific energy of the

particle, E. This conserved quantities are related, in the plane $z = 0$, by the expression

$$E = \frac{1}{2}\dot{\rho}^2 + \frac{\ell^2}{2\rho^2} + \psi, \tag{13}$$

where ψ is gravitational potential given by (7).

The orbit of the particle is found by solving the equations

$$\ddot{\rho} - \rho\dot{\varphi}^2 = -\frac{\partial\psi}{\partial\rho}, \tag{14}$$

$$\dot{\varphi} = \frac{\ell}{\rho^2}, \tag{15}$$

$$\dot{\rho}^2 = 2(E - V), \tag{16}$$

where $E \geq V$ and

$$V = \frac{\ell^2}{2\rho^2} + \psi, \tag{17}$$

is the effective potential, which can be written as

$$V = \frac{\ell^2}{2\rho^2} - m\frac{\pi}{2}, \tag{18}$$

for $0 \leq \rho \leq 1$, and as

$$V = \frac{\ell^2}{2\rho^2} - m\cot^{-1}\sqrt{\rho^2 - 1}, \tag{19}$$

for $\rho \geq 1$.

We begin by considering the above potential for radial orbits, when $\ell = 0$. So, as we can see form (18) and (19), the effective potential has a negative constant value at the interior of the disk and then monotonically increases to zero as $\rho \to \infty$. Accordingly, for $-m\pi/2 < E < 0$, the particle moves through the disk by oscillating into the circle of radius $\rho = \csc(-E/m)$. On the other hand, for $E \geq 0$, the particle moves along unbounded trajectories that go through the disk.

We now consider the behavior of the effective potential for non-radial orbits, when $\ell \neq 0$. As we can see from (18) and (19), at the interior of the disk the potential decreases as $1/\rho^2$, whereas at the exterior of the disk the behavior of the potential depends on the value of the specific angular momentum ℓ. So, in order to determine the nature of the possible non-radial orbits, we did a graphical analysis of the above potential for many values of the parameters. As an example, in Figure 1 we show the effective potential for $m = 1$ and three different values of ℓ

that show the three different behaviors of the effective potential V. For $\ell < \sqrt{2m}$, after the edge of the disk the potential increases monotonically to zero as $\rho \to \infty$. For $\ell > \sqrt{2m}$, after the edge of the disk the potential has two critical points, a maximum and a minimum, and after that the potential goes to zero as $\rho \to \infty$. Finally, when $\ell = \sqrt{2m}$, the two critical points collapse to only one and then the potential goes to zero as $\rho \to \infty$.

As we can see from the above analysis, exists a stable circular orbit at the edge of the disk, whereas at the exterior of the disk may exist two, one or no circular orbit by depending of the value of ℓ. We can find the radius of the external circular orbits by equalling to zero the first derivative of the effective potential with respect to ρ. So, as the effective potential at the exterior of the source can be written as (19), the external circular orbits has radius given by

$$\rho_{\pm}^2 = \frac{\ell^4}{2m^2} \pm \frac{\ell^2}{2m^2}\sqrt{\ell^4 - 4m^2}. \tag{20}$$

Accordingly, when $\ell > \sqrt{2m}$ we have two radius, one corresponding to the stable circular orbit, ρ_+, and the other to the unstable circular orbit, ρ_-. On the other hand, when $\ell = \sqrt{2m}$ we have only one radius, corresponding to the marginally stable orbit, and when $\ell < \sqrt{2m}$ we have not any circular orbit.

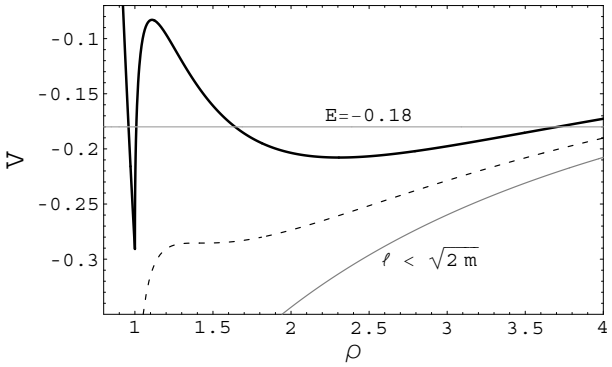

Figure 1. Newtonian effective potential V as a function of ρ for $m = 1$ and $\ell = 1.6$, $\ell = 1.4142$ and $\ell = 1$, from top to bottom.

We can also find the specific angular momentum of the particle in the external circular orbits by resolving for ℓ in the equation $V'(\rho) = 0$. Thus we obtain

$$\ell^2 = \frac{\rho^2 m}{\sqrt{\rho^2 - 1}}, \tag{21}$$

where we see that the specific angular momentum is always positive. Finally, we can use the above expression in order to find the radius of the marginally stable

orbit and obtain $\rho = \sqrt{2}$, by using the value $\ell = \sqrt{2m}$ in the equation (21). In Figure 1, the marginally stable orbit appears at the dotted curve.

Also, from the above considerations we can see that, when $\ell > \sqrt{2m}$ and for some values of the specific energy E, will exist two potential wells in such a way that bounded non-circular orbits are possible. In Figure 1 this situation is depicted for a specific energy $E = -0.18$, so we have two potential wells at the regions $0.959 \leq \rho \leq 1.031$ and $1.3 \leq \rho \leq 6.79$. Now, in order to have some example of the possible orbits, we must to solve the orbit equation. At the interior of the disk the orbit equation in polar coordinates is given by

$$\frac{d\rho}{d\varphi} = \pm\, \rho\, \sqrt{\alpha^2 \rho^2 - 1}, \tag{22}$$

where $\alpha^2 = 2(E - \psi)/\ell^2$. The above equation can be explicitely integrated and its solution can be written, in cartesian coordinates (x, y), as

$$\pm\alpha(\cos\varphi_0 x - \sin\varphi_0 y) = 1, \tag{23}$$

where φ_0 corresponds to the initial condition of the differential equation (22). On the other hand, at the exterior of the disk the motion equations must be solved numerically. In Figures 2 and 3 we show the bounded orbits corresponding to

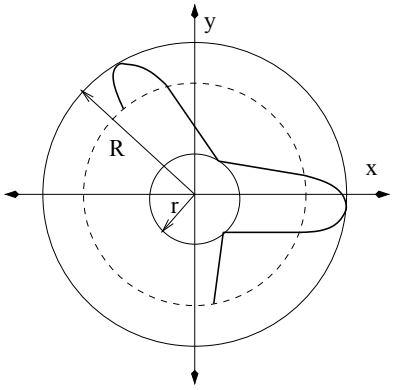

Figure 2. Example of bounded orbits for arbitrary initial conditions compatible with the first potential well in Figure 1. The motion of the particle is restricted to the region between $\rho = r = \alpha^{-1}$ and $\rho = R$. The dotted curve represents $\rho = 1$, the edge of the disk.

the two potential wells. In Figure 2 we show a portion of the orbit for the first potential well with an arbitrary initial condition. Then, in Figure 3 we present a portion of the orbit for the potential well at the region $1.64 \leq \rho \leq 3.7$, with $\ell = 1.6$ and $E = -0.18$.

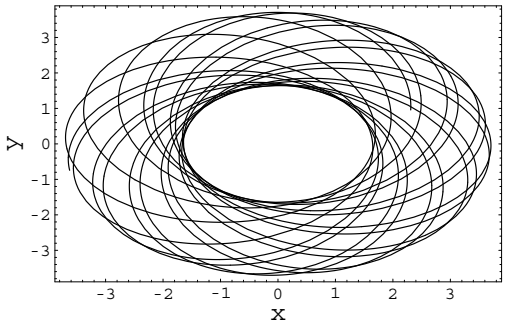

Figure 3. Example of bounded orbits for the second potential well in Figure 1 with $m = 1$, $\ell = 1.6$ and $E = -0.18$. The orbit is confined to the region between $\rho \approx 1.64$ and $\rho \approx 3.7$.

4. The Relativistic motion

We now analyze the motion of test particles in the equatorial plane of the relativistic thin disk defined by (7) and (8). In order to do this, we define the Lagrangian $\mathcal{L}$ through the relation

$$2\mathcal{L} = -e^{2\psi}\dot{t}^2 + e^{-2\psi}[\rho^2\dot{\varphi}^2 + e^{2\gamma}(\dot{\rho}^2 + \dot{z}^2)], \tag{24}$$

where $\dot{x}^\alpha$ are the derivatives with respect to the affine parameter τ, so that we have two conserved quantities,

$$E = e^{2\psi}\dot{t}, \tag{25}$$

$$\ell = e^{-2\psi}\rho^2\dot{\varphi}, \tag{26}$$

corresponding, respectively, to the specific energy and specific azimuthal angular momentum of the particle with respect to a rest frame at infinity. Now, by considering motion at the equatorial plane, the differential equation for the radial coordinate ρ can be written as

$$\dot{\rho}^2 = e^{-2\gamma}\left[E^2 + \epsilon\, e^{2\psi} - \frac{\ell^2 e^{4\psi}}{\rho^2}\right], \tag{27}$$

where $\epsilon = 2\mathcal{L}$, and thus $\epsilon = -1$ for timelike geodesics and $\epsilon = 0$ for null geodesics. In order to do a qualitative analysis of the behavior of the geodesics, the differential equation for the radial coordinate can be cast as $\frac{\dot{\rho}^2}{2} + V(\rho) = \mathcal{E}$, where the total effective energy $\mathcal{E}$ has only the value $\mathcal{E} = 0$ and the effective potential $V(\rho)$ is given by

$$V(\rho) = \frac{e^{-2\gamma}}{2}\left[\frac{\ell^2 e^{4\psi}}{\rho^2} - E^2 - \epsilon e^{2\psi}\right], \tag{28}$$

so that the motion is only possible when $V(\rho) < 0$.

We consider, in first instance, the motion of radial geodesics, when $\ell = 0$. The effective potential can be written as

$$V(\rho) = -\left[\frac{1}{1-\rho^2}\right]^{m^2}\left[\frac{\epsilon e^{-m\pi} + E^2}{2}\right], \tag{29}$$

for $0 \leq \rho < 1$, and

$$V(\rho) = -\left[\frac{\rho^2}{\rho^2-1}\right]^{m^2}\left[\frac{\epsilon e^{-2m\cot^{-1}\sqrt{\rho^2-1}} + E^2}{2}\right], \tag{30}$$

for $\rho > 1$. As we can see from the above expressions, for radial null geodesics the potential decreases monotonically from a finite negative value at the center of the disk, has a negative singularity at the rim of the disk, and then increases monotonically from the singularity and goes asymptotically to a finite negative value at infinity. Accordingly, as the total effective energy is zero, we can conclude that the only possible kind of radial null geodesics are unbounded trajectories that go through the disk.

On the other hand, for radial timelike geodesics, the potential will be always negative only if $E^2 \geq 1$ and, in this case, the behavior of the potential is like for the null geodesics. However, if $e^{-m\pi} < E^2 < 1$, after the negative singularity at the rim of the disk the potential increases monotonically and goes asymptotically to a finite positive value at infinity. Accordingly, the particle moves through the disk by oscillating into the circle of radius $\rho^2 = 1 - \cot(2m \ln E^2)$. Finally, if $E^2 \leq e^{-m\pi}$, the potential will be everywhere positive and thus the motion is not possible.

Now we consider the motion of non-radial geodesics in such a way that, as $\ell \neq 0$, the effective potential is given by

$$V(\rho) = \left[\frac{1}{1-\rho^2}\right]^{m^2}\left[\frac{\ell^2 e^{-2m\pi}}{2\rho^2} - \frac{\epsilon e^{-m\pi} + E^2}{2}\right], \tag{31}$$

for $0 \leq \rho < 1$, and

$$V(\rho) = \left[\frac{\rho^2}{\rho^2-1}\right]^{m^2}\left[\frac{\ell^2}{2\rho^2}e^{-4m\cot^{-1}\sqrt{\rho^2-1}} - \frac{\epsilon}{2}e^{-2m\cot^{-1}\sqrt{\rho^2-1}} - \frac{E^2}{2}\right], \tag{32}$$

for $\rho > 1$. As we can see, as much for timelike and null geodesics, the potential goes to infinity as ρ goes to zero and then decreases monotonically until a negative

singularity at the rim of the disk. Now, the condition that $V(\rho) < 0$ implies that the motion is only possible for $\rho > \rho_{min}$, where

$$\rho_{min}^2 = \frac{\ell^2 e^{-2m\pi}}{E^2 + \epsilon e^{-m\pi}}, \tag{33}$$

and then we can choose the values of the constants in such a way that $0 < \rho_{min} < 1$.

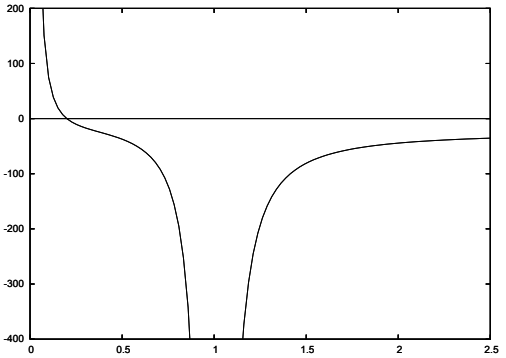

Figure 4. The effective potential V as a function of ρ for non-radial null geodesics with $m = \sqrt{2}$, $E = 5$ and $\ell^2 = 1.87 \times 10^{-3}$.

On the other hand, after the rim the behavior of the potential is different for timelike or null geodesics. For null geodesics the potential after the rim increases monotonically from the singularity and goes asymptotically to a finite negative value at infinity. An example of the found behavior is depicted in Figure 4, where we plot the effective potential as a function of ρ for non-radial null geodesics with $m = \sqrt{2}$, $E = 5$ and $\ell^2 = 1.87 \times 10^{-3}$. In concordance with the above behavior, we conclude that the non-radial null geodesics are unbounded orbits. The particles come from infinity until they reach the turning point, at $\rho = \rho_{min}$, and then return to infinity.

For timelike geodesics, on the other hand, after the rim of the disk the behavior of the potential depends on the value of the specific angular momentum. So, in order to see the possible kinds of behavior, we did a graphical analysis of the potential for many values of the parameters. As an example, we show in Figure 5 the effective potencial for non-radial timelike geodesics with $m = 1$ and $E = 1$. As we can see, there are three kinds of behavior. For some values of ℓ the potential behaves like for the null geodesics, as we can see at the curve labeled (b) in Figure 5, and so the possible orbits are similar to the non-radial null geodesics.

For some other values of ℓ the potential increases from the singularity at the rim until a local positive maximum and then decreases to a finite negative value as ρ

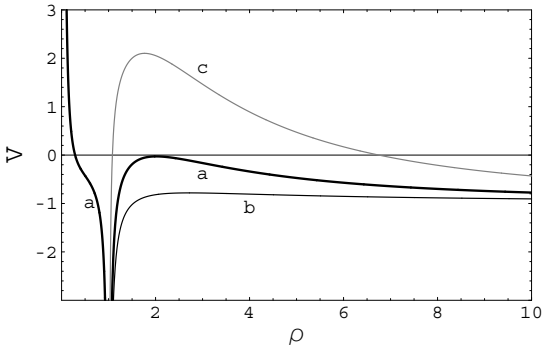

Figure 5. The effective potential V as a function of ρ for non-radial timelike geodesics with $m = 1$ and $E = 1$. In (a) $\ell \approx 6.52$, in (b) $\ell = 2$, and in (c) $\ell = 12$.

goes to infinity, as is shown at the curve labeled (c) in Figure 5. So, as the total effective energy is zero, we have two allowed regions: a well of potential around the rim of the disk, where we have bounded orbits, and an external region, where we have unbounded trajectories similar to the non-radial null geodesics. Finally, there are some value of ℓ for which the local maximum of the potential is equal to zero, as happen at the curve labeled (a) in Figure 5, in which case we have an unstable circular orbit. We can find the values of the specific energy, E, and the specific angular momentum, ℓ, for the unstable circular orbit by solving the system of equations $V(\rho) = 0$ and $V'(\rho) = 0$, and thus we obtain

$$E^2 = \frac{[\sqrt{\rho^2-1} - m]e^{-2m\cot^{-1}\sqrt{\rho^2-1}}}{2m - \sqrt{\rho^2-1}}, \tag{34}$$

$$\ell^2 = \frac{m\rho^2 e^{2m\cot^{-1}\sqrt{\rho^2-1}}}{2m - \sqrt{\rho^2-1}}, \tag{35}$$

where $1 + m^2 \leq \rho^2 \leq 4m^2 + 1$.

Now, in order to have some examples of the possible non-radial geodesics, we must to solve the orbit equation. The differential equation of the orbit can be written as

$$d\varphi = \pm\frac{\rho_{min}}{\rho}\left[\frac{(1-\rho^2)^{m^2}}{\rho^2 - \rho_{min}^2}\right]^{\frac{1}{2}} d\rho, \tag{36}$$

for $0 \leq \rho < 1$, and as

$$d\varphi = \pm\frac{\ell}{\rho^2}\left[\frac{(\rho^2-1)^{m^2}}{(E^2 + \epsilon e^{2\psi})\, e^{-4\psi}\rho^2 - \ell^2}\right]^{\frac{1}{2}} d\rho, \tag{37}$$

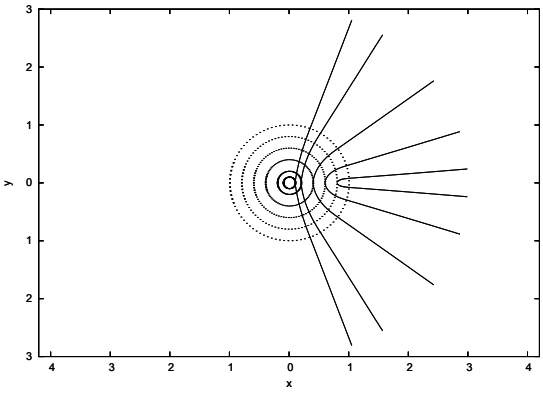

Figure 6. Example of orbits for non-radial null geodesics with $m = \sqrt{3}$ in cartesian coordinates, (x, y). For the orbit with $\rho_{min} = 0.1$ we take $E = 10$, whereas for the orbits with $\rho_{min} = 0.2$, 0.4, 0.6 and 0.8 we take $E = 5$.

for $\rho > 1$, where $\psi = -m \cot^{-1} \sqrt{\rho^2 - 1}$. So, when we numerically solve the above equations for the non-radial timelike geodesics with values of E and ℓ similar to the used in the curve labeled (c) in Figure 5, and with initial conditions corresponding to the well of potential around the rim of the disk, we find orbits that resemble to the presented in the Newtonian case and illustrated at Figure 2.

As we can see from the behavior of the potential, in any other case different from the above, the non-radial geodesics are unbounded orbits with similar behavior for the null case and for the timelike case. So, in order to have an example of the unbounded orbits, we numerically solve the orbit equation for non-radial null geodesics with the initial condition $\varphi(\rho_{min}) = 0$. In Figure 6 we show some example of orbits for non-radial null geodesics with $m = \sqrt{3}$. For the orbit with $\rho_{min} = 0.1$ we take $E = 10$, whereas for the orbits with $\rho_{min} = 0.2$, 0.4, 0.6 and 0.8 we take $E = 5$. For many other values of m, E and ρ_{min}, the plots of the orbits present a similar behavior, as much for the case of null geodesics as for the case of time-like geodesics.

5. Concluding remarks

We presented a study of timelike and null equatorial geodesics in the Bonnor-Sackfield relativistic thin disk, the first member of the Morgan-Morgan family of thin disks. We analyzed the motion of test particles in the gravitational field generated for the relativistic thin disk and also in the corresponding newtonian thin disk. The nature of the possible orbits was studied by means of a qualitative analysis of the effective potential and by numerically solving the motion equation,

both for radial and for non-radial equatorial trajectories.

For the case of radial motion we found a similar behavior of the relativistic timelike geodesics with the newtonian motion, presenting bounded as unbounded radial trajectories, whereas the possible radial null geodesics only are unbounded trajectories. Now, for the case of non-radial motion, we find similar behavior for the relativistic and for the newtonian case. However, some differences exist. Stable circular orbits only exist in the newtonian case whereas for the relativistic case can only exist a unstable circular orbit for some values of the parameters. We computed the specific energy, specific angular momentum and radius of the circular orbits both for the relativistic and newtonian motion.

We presented some examples of the numerical results, obtained with some simple values of the parameters; however, we compute the solutions for many other values of these and found similar behavior in all the cases. Furthermore, although the differential equations are different for timelike and null geodesics, as for the newtonian case, we found similar qualitative characteristics in many of the considered cases.

References

[1] Bateman H., *Higher Transcendental Functions*, McGraw Hill, New York, vol 1. 1953.

[2] Bičák J. and Ledvinka T., "Relativistic disks as sources of the Kerr metric", *Phys. Rev. Lett.* 71 (1993), no. 11, 1669–1672.

[3] Bičák J., Lynden-Bell D. and Katz J., "Relativistic disks as sources of static vacuum spacetimes", *Phys. Rev. D* 47 (1993), 4334–4343.

[4] Bičák J., Lynden-Bell D. and Pichon C., "Relativistic discs and flat galaxy models", *Monthly Notice Roy Astronom. Soc.* 265 (1993), no. 1, 126–144.

[5] Bonnor W.A. and Sackfield A., "The interpretation of some spheroidal metrics", *Comm. Math. Phys.* 8 (1968), no. 4, 338–344.

[6] D'Afonseca L.A., Letelier P.S., and Oliveira S.R., "Geodesics around Weyl-Bach's ring solution", *Class. Quantum Grav.* 22 (2005), no. 17, 3803–3814.

[7] González G. and Espitia O.A., "Relativistic static thin disks: The counterrotating model", *Phys. Rev. D* 68 (2003), no. 10, 104028-1 – 104028-8.

[8] González G. and Letelier P.S., "Rotating relativistic thin disks", *Phys. Rev. D* 62 (2000), 064025-1 – 064025-8.

[9] González G. and Letelier P.S., "Relativistic static thin discs with radial stress support", *Class. Quantum Grav.* 16 (1999), no. 2, 479–494.

[10] Kramer D., Stephani H., Herlt E. and McCallum M., *Exact Solutions of Einsteins's Field Equations*, Cambridge University Press, Cambridge-England, 2000.

[11] Lemos J.P.S., "Self-similar relativistic discs with pressure", *Class. Quantum Grav.* 6 (1989), no. 9, 1219–1230.

[12] Lemos J.P.S. and Letelier P.S., "Superposition of Morgan and Morgan discs with a Schwarzschild black hole", *Class. Quantum Grav.* 10 (1993), no. 6, L75–L78.

[13] Lemos J.P.S. and Letelier P.S., "Exact general relativistic thin disks around black holes", *Phys. Rev. D* 49 (1994), 5135–5143.

[14] Lemos J.P.S. and Letelier P.S., "Two families of exact disks with a central black hole", *Int. J. Modern Phys. D* 5 (1996), no. 1, 53–63.

[15] Letelier P.S. and Oliveira S.R., "Exact selfgravitating disks and rings: a solitonic approach", *J. Math. Phys.* 28 (1987), no. 1, 165–170.

[16] Lynden-Bell D. and Pineault S., "Relativistic disks - 1. Counter rotating disks", *Monthly Notice Roy Astronom. Soc.* 185 (1978), 679–694.

[17] Lynden-Bell D. and Pineault S., "Relativistic disks - 11. Self-similar disks in rotation", *Monthly Notice Roy Astronom. Soc.* 185 (1978), 695–712.

[18] Morgan T. and Morgan L., "The Gravitational Field of a Disk", *Phys. Rev.* 183 (1969), 1097–1101.

[19] Morgan L. and Morgan T., "Gravitational Field of Shells and Disks in General Relativity", *Phys. Rev. D* 2 (1970), 2756–2761.

[20] Morse P.M. and Feshbach H., *Methods of Theoretical Physics*, McGraw-Hill, New York, 1953.

[21] Semerák O., "Gravitating discs around a Schwarzschild black hole. III", *Class. Quantum Grav.* 20 (2003), no. 9, 1613–1634.

[22] Semerák O. and Žáček M., "Oscillations of static discs around Schwarzschild black holes: Effect of self-gravitation", *Publ. Astron. Soc. Japan* 52 (2000), 1067–1074.

[23] Semerák O., Žáček M. and Zellerin T., "The structure of superposed Weyl fields", *Monthly Notice Roy Astronom. Soc.* 308 (1999), 691–704.

[24] Voorhees B.H., "Static Axially Symmetric Gravitational Fields", *Phys. Rev. D* 2 (1970), 2119–2122.

[25] Weyl H., "Ausbreitung elektromagnetischer Wellen über einem ebenen Leiter", *Ann. Physik* 54 (1917), 117–145.

[26] Weyl H., "Bemerkung über die axialsymmetrischen Lösungen der Einsteinschen Gravitationsgleichungen", *Ann. Physik* 59 (1919), 185–189.

[27] Zipoy D.M., "Topology of Some Spheroidal Metrics", *J. Math. Phys.* 7 (1966), 1137–1143.